Supporting Information for

Buckling in serpentine microstructures and applications in elastomer-supported ultra-stretchable electronics with high areal coverage

Yihui Zhang[1,2,†], Sheng Xu[3,†], Haoran Fu[1,4], Juhwan Lee[3], Jessica Su[3], Keh-Chih Hwang[2,5], John A. Rogers[3,*] and Yonggang Huang[1,6,7*]

[1]Department of Civil and Environmental Engineering and Department of Mechanical Engineering, Northwestern University, Evanston, IL 60208, USA

[2]Center for Mechanics and Materials, Tsinghua University, Beijing 100084, China

[3]Department of Materials Science and Engineering, Frederick Seitz Materials Research Laboratory, University of Illinois at Urbana-Champaign, Urbana, Illinois 61801, USA

[4]Department of Civil Engineering, Zhejiang University, Hangzhou, 310058, China

[5]AML, Department of Engineering Mechanics, Tsinghua University, Beijing 100084, China

[6]Institute of Public Health and Medicine, Northwestern University, Evanston, IL 60208, USA

[7]Skin Disease Research Center, Feinberg School of Medicine, Northwestern University, Evanston, IL 60208, USA

†These authors contributed equally to this work

Correspondence and requests for materials should be addressed to Y.G.H. (email: y-huang@northwestern.edu) or to J.A.R. (email: jrogers@illinois.edu).

Keywords: Stretchable electronics; Mechanical properties; Serpentine interconnect; Buckling analyses; Modeling

1. The effective flexibility and critical buckling strain of serpentine interconnect

We consider a serpentine interconnect subject an axial force N (along the direction between the two ends of the interconnect), a shear force Q (normal to N), and a bending moment M, at the right end, within the plane of interconnect, as shown in **Fig. S1**. The width and thickness of the serpentine interconnect are usually much smaller than the length such that the structure can be modeled as a curved beam.

We first determine the effective flexibility (or stiffness) of the serpentine interconnect. Let u and w denote the displacements at the right end, along and normal to the axial direction of the interconnect (parallel to N and Q), respectively, and θ is the rotational angle (**Fig. S1**). They are related to (N, Q, M) via the strain energy W in the interconnect by

$$\begin{Bmatrix} u \\ w \\ \theta \end{Bmatrix} = \begin{Bmatrix} \partial W/\partial N \\ \partial W/\partial Q \\ \partial W/\partial M \end{Bmatrix} = \begin{bmatrix} T_{11} & T_{12} & T_{13} \\ T_{12} & T_{22} & T_{23} \\ T_{13} & T_{23} & T_{33} \end{bmatrix} \begin{Bmatrix} N \\ Q \\ M \end{Bmatrix} = \boldsymbol{T} \begin{Bmatrix} N \\ Q \\ M \end{Bmatrix}, \tag{S1}$$

where W is a quadratic function of N, Q, and M for linear elastic behavior of the interconnect, which is the sum of strain energy in all unit cells; and $\boldsymbol{T}$ is the symmetric flexibility matrix of the serpentine interconnect to be determined.

The free body diagram for the k^{th} unit cell is shown in the **Fig. S1**. Its strain energy in the k^{th} unit cell, $W_{(k)}$, is obtained from the summation of bending energy in all straight and curved parts as

$$W_{(k)} = \frac{l_1^3}{48EI_3} \begin{Bmatrix} N^2\left(3\pi + 24\alpha + 6\pi\alpha^2 + 4\alpha^3\right) + 3Q^2\left(3\pi + 8\alpha\right) + 12QN\left(2 + \pi\alpha + \alpha^2\right) \\ +24\left(\pi + 2\alpha\right)\left[\left(M/l_1\right) + Q\left(2m - 2k + 1\right)\right]^2 \end{Bmatrix}, \tag{S2}$$

where $EI_3=Ew^3t/12$ is the in-plane bending stiffness of the serpentine interconnect. This gives the strain energy of the serpentine interconnect $W = \sum_{k=1}^{m} W_{(k)}$. The components of the flexibility matrix for the serpentine interconnect can be then determined from Eq. (S1) as

$$
\begin{aligned}
T_{11} &= \frac{ml_1^3}{24EI_3}\left(3\pi + 24\alpha + 6\pi\alpha^2 + 4\alpha^3\right), \\
T_{22} &= \frac{ml_1^3}{24EI_3}\left[\pi\left(32m^2+1\right) + 8\left(8m^2+1\right)\alpha\right], \\
T_{33} &= \frac{ml_1}{EI_3}\left(\pi + 2\alpha\right), \\
T_{12} &= T_{21} = \frac{ml_1^3}{4EI_3}\left(2 + \pi\alpha + \alpha^2\right), T_{23} = T_{32} = \frac{m^2 l_1^2}{EI_3}\left(\pi + 2\alpha\right), T_{31} = T_{13} = 0
\end{aligned}
\quad . \tag{S3}
$$

For stretching of serpentine interconnect, $u=u_0$, $w=0$ and $\theta=0$, the reaction force (N) along the axial direction is given by

$$
N = \frac{T_{23}^2 - T_{22}T_{33}}{T_{11}T_{23}^2 + T_{33}T_{12}^2 - T_{11}T_{22}T_{33}} u_0 \, . \tag{S4}
$$

This, together with the critical buckling load in Eq. (1) gives the critical buckling strain in Eq. (3).

2. Numerical simulations on the critical buckling and postbuckling behavior

Three-dimensional finite element method (FEM) was adopted to analyze the critical buckling and postbuckling behavior of the serpentine interconnect. Four-node shell elements were used to model the interconnect, and the refined meshes were adopted to ensure the accuracy. The serpentine interconnect made of gold was analyzed to establish the scaling laws of critical buckling strain and elastic stretchability (**Figs. 2 and 5**), particularly their dependences on the geometric parameters. The serpentine interconnect was composed of three layers, i.e., a metal layer (e.g., copper) encased, top and bottom, by two polyimide (PI) layers in the study of postbuckling processes (**Figs. 4 and 6**), in order to accord with the experiments. These two PI layers were adopted in experiment to avoid possible short circuits during stretching. The material parameters (elastic modulus E and Poisson's ratio v) used in the simulations include E_{Cu}=119 GPa and v_{Cu}=0.34 for copper; E_{Au}=78 GPa and v_{Au}=0.44 for gold; and E_{PI}=2.5 GPa and v_{PI}=0.34 for PI.

We used FEM to determine three functions $f_1(m)$, $f_2(m)$, and $f_3(m)$ in Eqs. (1) to (3) for the critical buckling strain, as described in Section 2.1. Here, we fixed the cross section aspect ratio (t/w), as 1/20, and adopted three different length/spacing aspect ratios (e.g., α=2, 5, and 7) for the serpentine interconnect to determine $f_1(m)$, $f_2(m)$, and $f_3(m)$ for different number (m) of unit cells. The functions ($f_1(m)$, $f_2(m)$, and $f_3(m)$) were determined separately for the symmetric and anti-symmetric buckling modes. For the symmetric mode (which only occurs when m=1), f_1=0.276, f_2=1.05 and f_3=0.358, respectively. For the anti-symmetric mode, $f_1(m)$, $f_2(m)$, and $f_3(m)$ are shown in **Table S1**. These $f_1(m)$, $f_2(m)$ and $f_3(m)$, determined from a single cross section aspect ratio (t/w) and three different length/spacing aspect ratios (α), predicted well the critical buckling strains for a very wide range of t/w (from 0.0125 to 0.3), and α (from 1 to 9), as shown in **Fig. 2**. As shown in **Fig. 2a**, a wide range of thickness and width were adopted in simulations.

SI Tables

Table S1. The functions $f_1(m)$, $f_2(m)$ and $f_3(m)$ for different number of unit cell m.

m	1	2	3	4	5	6	7	8
$f_1(m)$	4.83	1.10	0.43	0.79	2.24	3.83	4.50	5.00
$f_2(m)$	-3.48	2.52	3.40	2.35	0.10	-2.23	-3.46	-4.40
$f_3(m)$	1.41	2.60	2.55	3.25	4.12	4.90	5.43	5.83

Table S2. The function $g_1(m,\alpha)$ for different length/spacing ratio α and number of unit cell m.

α \ M	1	2	3	4	5	$m\geq6$
0.5	1.935	1.805	1.567	1.541	1.502	1.466
1	1.516	1.163	1.018	0.979	0.954	0.928
2	0.893	0.514	0.532	0.506	0.491	0.478
3	0.583	0.333	0.338	0.331	0.307	0.296
4	0.413	0.249	0.237	0.219	0.208	0.201
5	0.311	0.184	0.172	0.157	0.149	0.144
7	0.196	0.111	0.0970	0.0867	0.0812	0.0793
9	0.129	0.0716	0.0594	0.0516	0.0494	0.0470

Table S3. The function $g_2(m,\alpha)$ for different length/spacing ratio α and number of unit cell m.

α \ m	1	2	3	4	5	$m\geq6$
0.5	12.51	3.46E-1	1.41E-1	8.92E-2	7.00E-2	6.44E-2
1	2.86	6.70E-2	1.39E-2	8.51E-3	6.72E-3	6.31E-3
2	1.89E-2	5.70E-3	3.30E-3	2.32E-3	1.99E-3	1.89E-3
3	5.91E-3	2.08E-3	1.41E-3	1.27E-3	1.42E-3	1.48E-3
4	2.06E-3	1.08E-3	8.98E-4	9.91E-4	1.07E-3	1.08E-3
5	1.22E-3	6.86E-4	7.48E-4	7.94E-4	8.04E-4	8.16E-4
7	6.33E-4	4.90E-4	4.79E-4	4.71E-4	4.67E-4	4.58E-4
9	4.93E-4	3.54E-4	3.18E-4	2.94E-4	2.94E-4	2.80E-4

SI Figure Captions

Figure S1. The serpentine interconnect with left end clamped, and right end subject to an axial force (N), a shear force (Q), and a bending moment (M), and the free body diagram of the $(k)^{th}$ unit cell.

Figure S2. The critical buckling strains of both symmetric and anti-symmetric modes as functions of aspect ratio, for the unit cell number of m=1 (a) and m=2 (b).

Figure S3. The maximum principal strain versus normalized thickness (a) and width (b), for different applied strains. The geometric parameters are m=1, α=3, and w/l_1=0.2 for (a) and t/l_1=0.01 for (b).

Figure S4. Functions F_1 (a) and F_2 (b), which show linear proportions of F_1 and F_2 to the square root of applied strain, and the square of applied strain, respectively.

Figure S5. Illustration of the dimensions for the optimized island bridge structure (**Fig. 6**) with high areal coverage of active device and large stretchability of overall system. The length unit is (mm) in the figure.

Figure S6. Design of selective bonding (a) or surface relief structure (b) for island structure to avoid large strain in device and substrate under stretching. The length unit is (mm) in the figure.

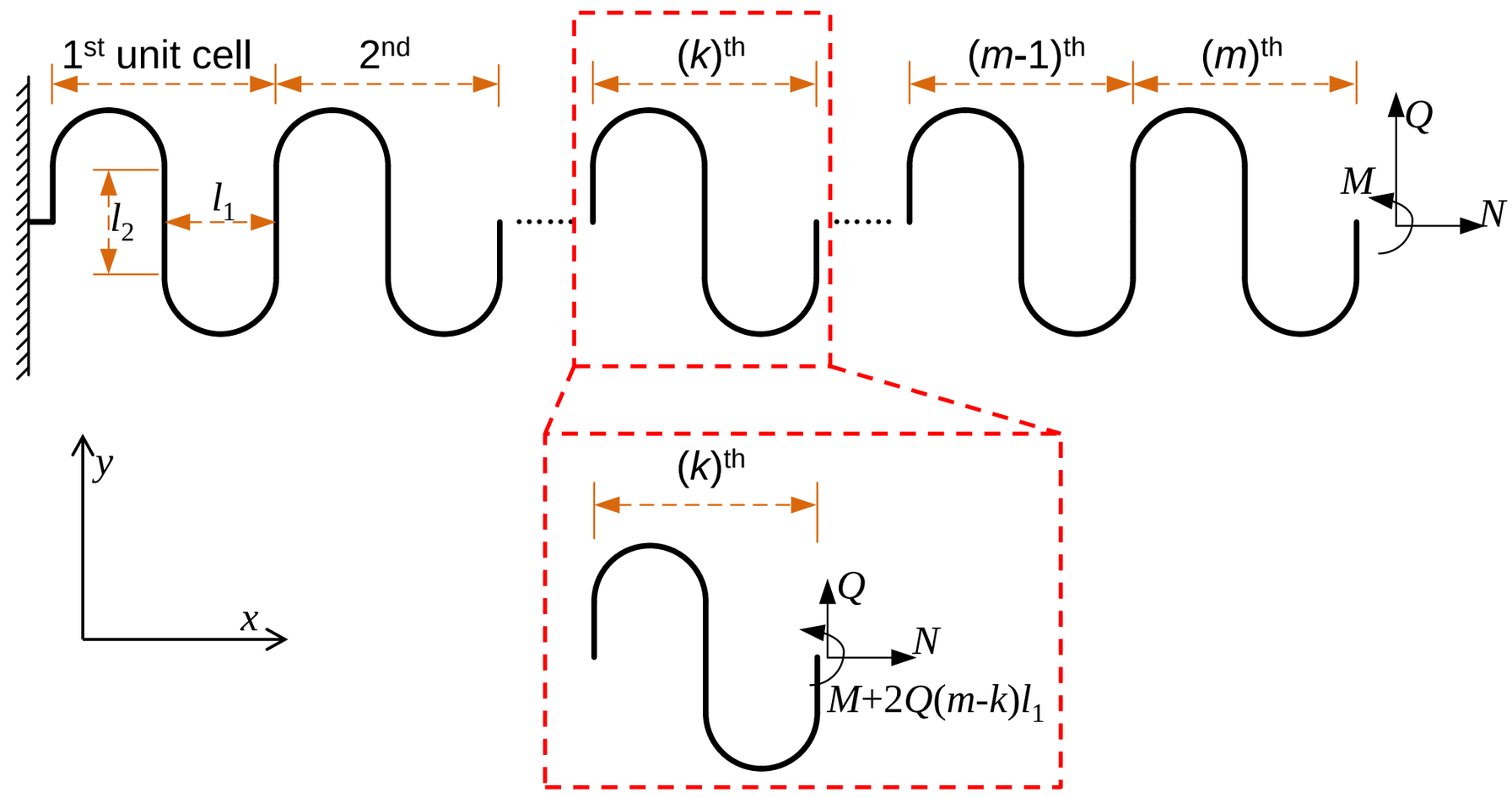

Figure S1

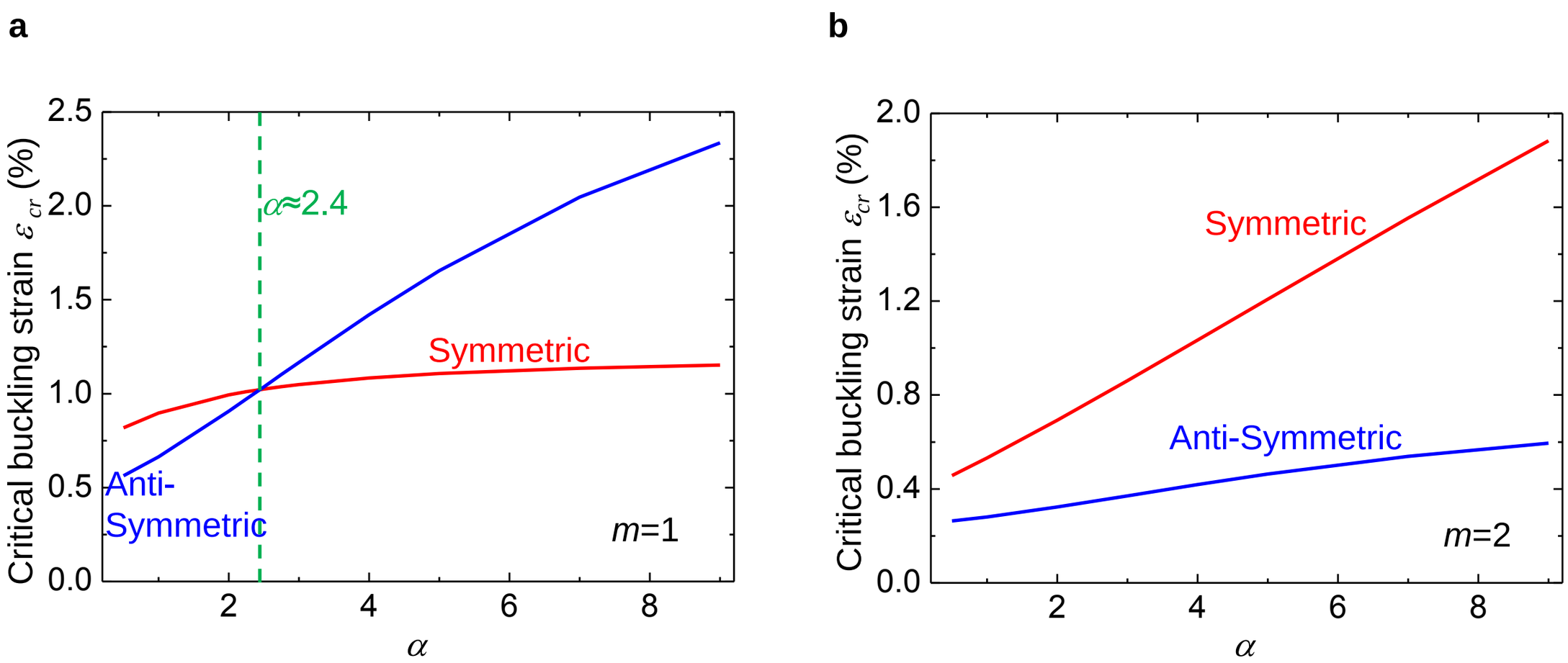

Figure S2

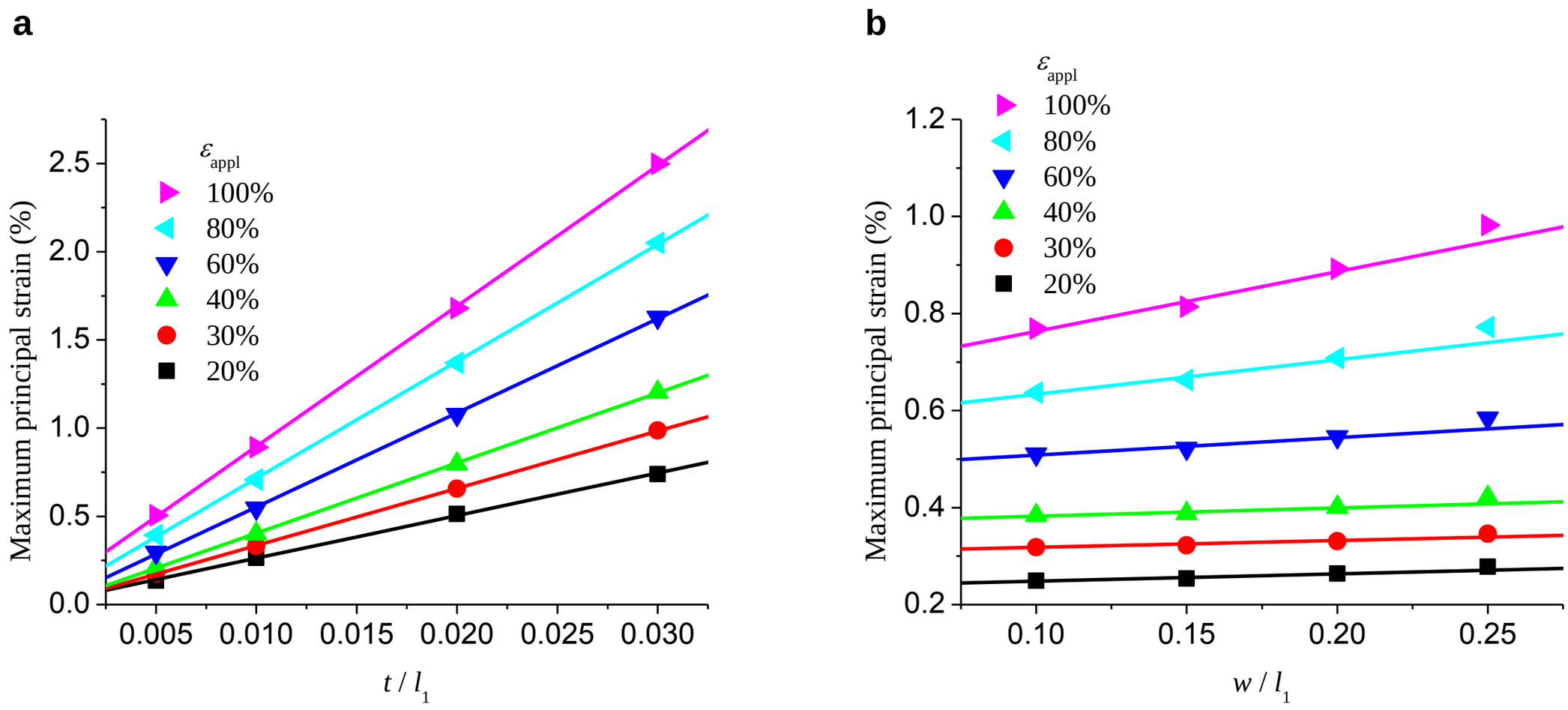

Figure S3

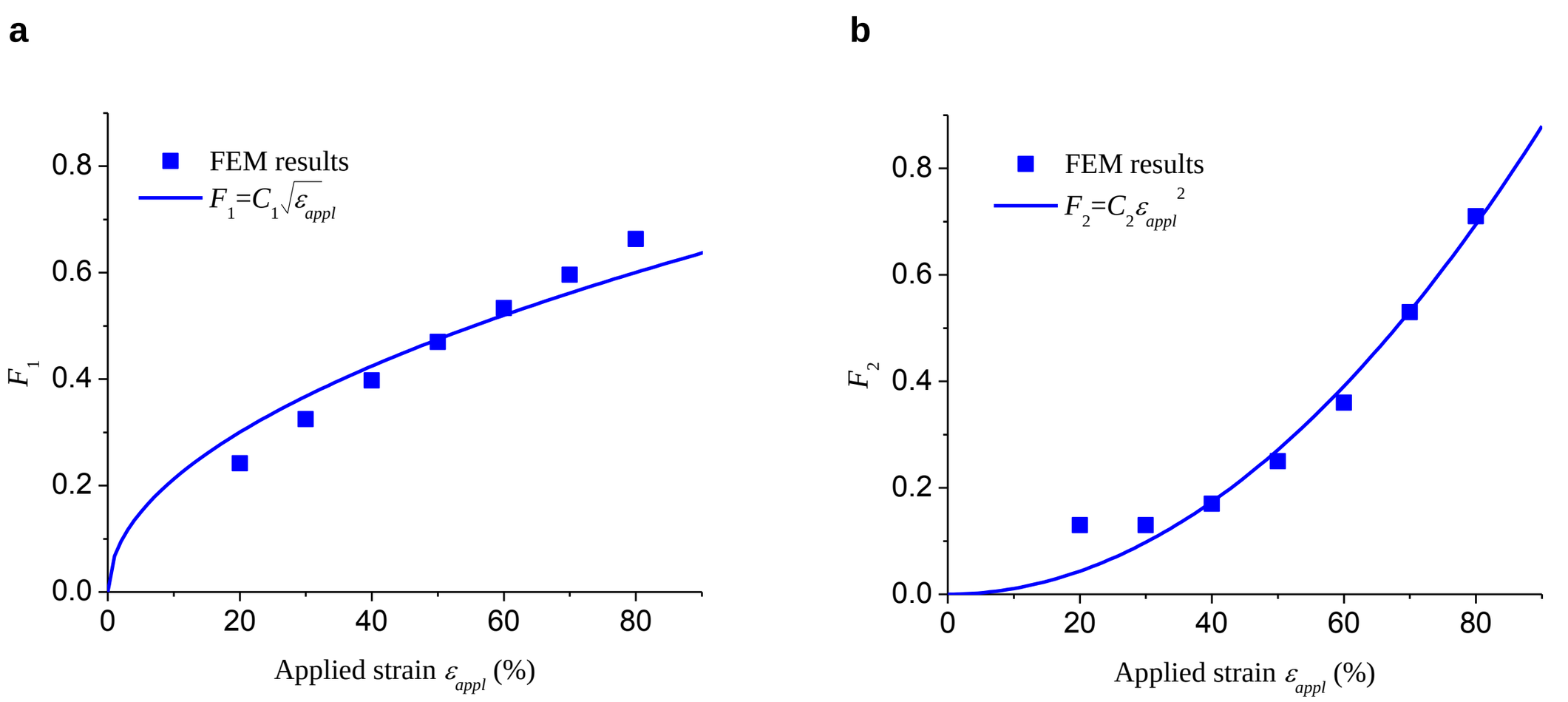

Figure S4

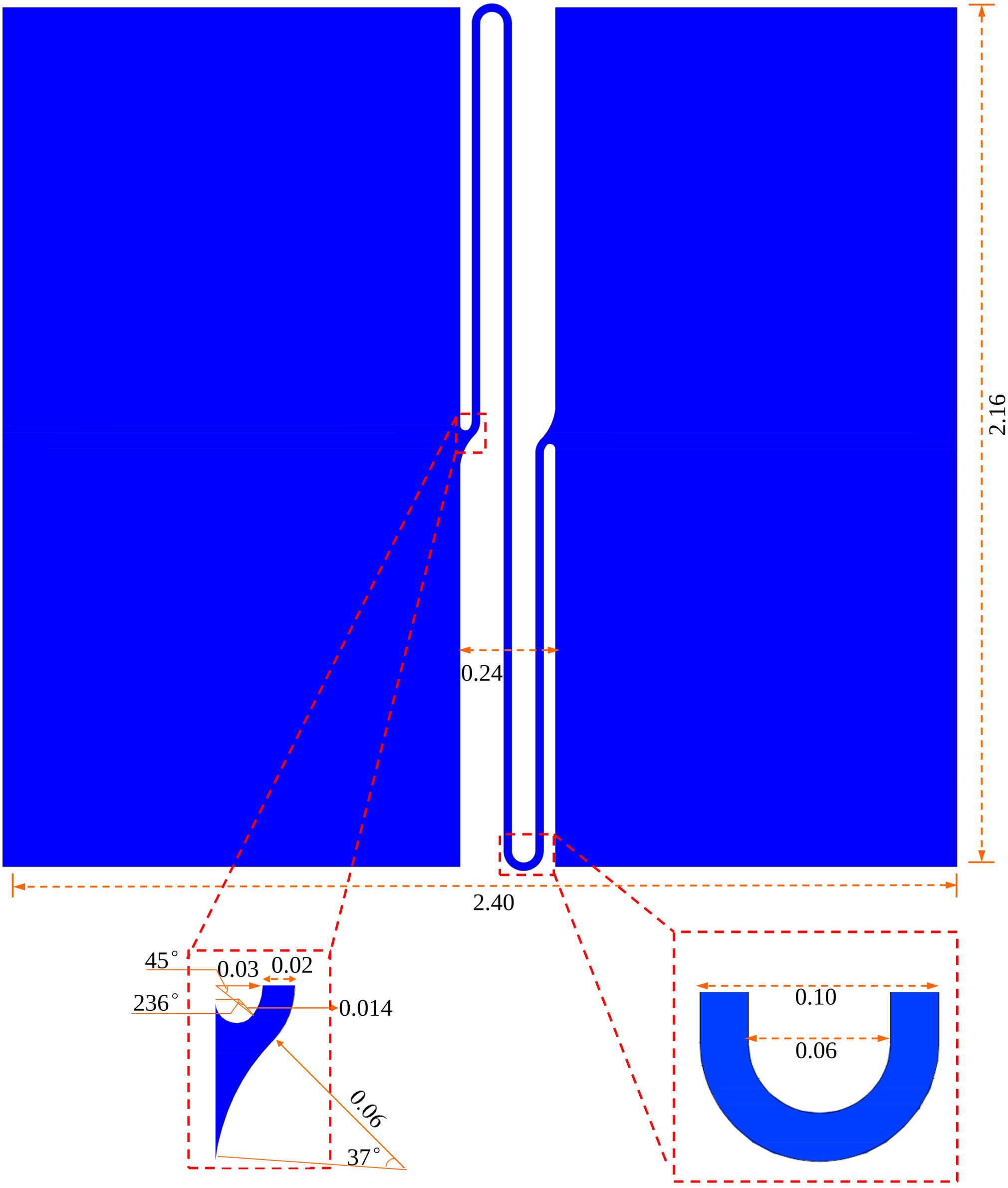

Figure S5

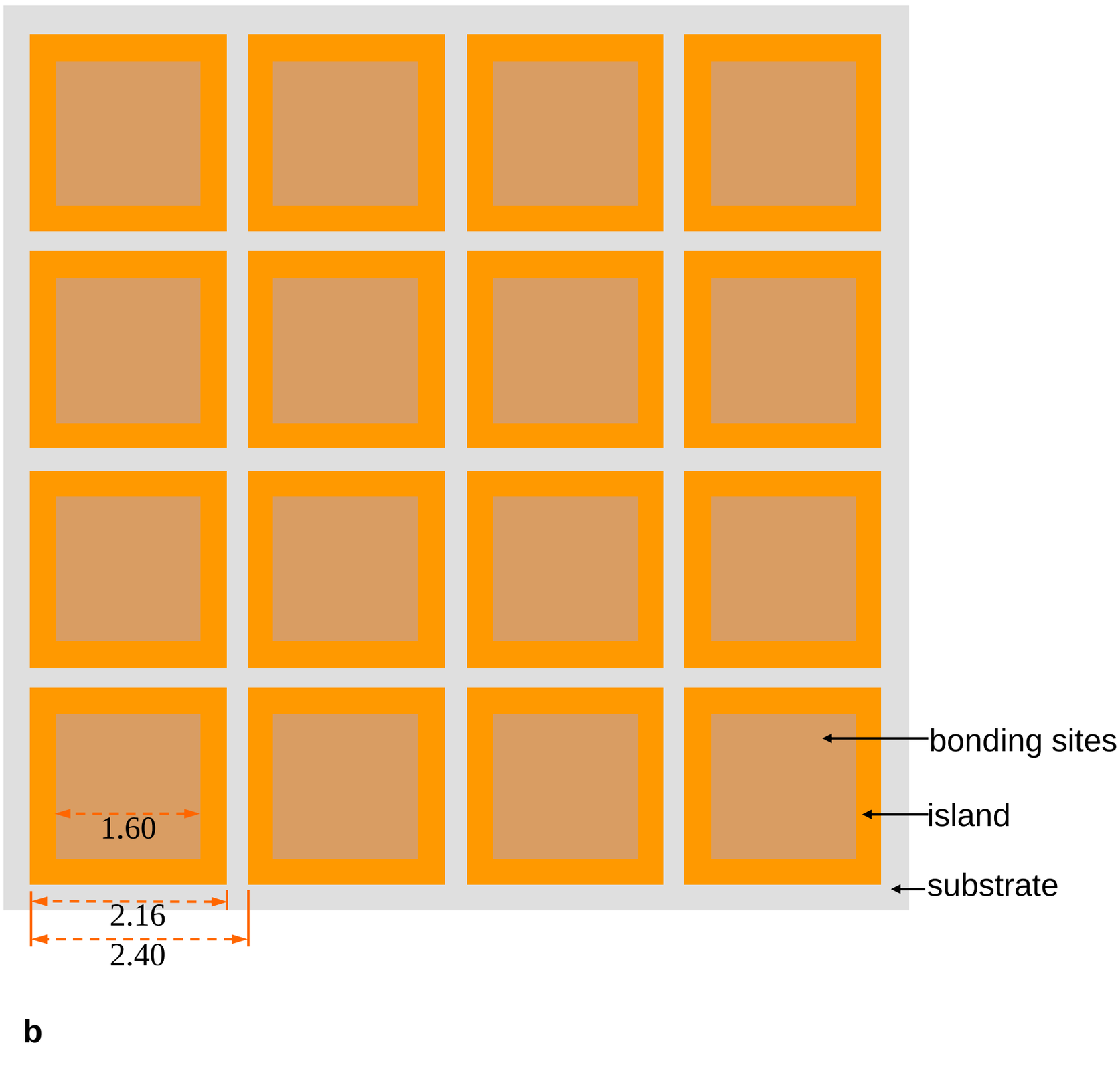

Figure S6